Theory onf brached growth

Thomas C. Halsey and Michael Leibig
The James Franck Institute and Department of Physics, The University of Chicago, 5640 South Ellis Avenue, Chicago, Illinois 60637
(Received 6 May 1992)

We present a theory of branched growth processes, notably diffusion-limited aggregation (DLA). Using a simple model of the dynamics of screening of competing branches, we compute statistics of the growth probability distribution. These statistics are multifractal only for stochastic models. Applying this general approach to diffusion-limited aggregation, we obtain results for the dimension D of a DLA cluster that are extremely close to the Muthukumar formula, $D=(d^2+1)/(d+1)$, in spatial dimensionality d [Phys. Rev. Lett. **50**, 839 (1983)]. This formula is believed to be accurate for DLA clusters in dimensions $d>2$. The maximum growth probability of the cluster scales as $p_{\max}\sim r^{1-D}$, with r the cluster radius, as predicted by Turkevich and Scher [Phys. Rev. Lett. **55**, 1026 (1985); Phys. Rev. A **33**, 786 (1986)]. We also discuss the scaling of the minimum growth probability, the behavior of nonstochastic models, and possible approaches to direct computation of the screening dynamics. Our results are in good qualitative, and in some cases good quantitative, agreement with numerical studies of the screening dynamics.

PACS number(s): 68.70.+w, 64.60.Ak, 05.20.−y

I. INTRODUCTION

Over ten years ago, Witten and Sander discovered that diffusion-limited aggregation (DLA) leads to highly branched, fractal structures [1]. Although some theoretical progress has been made, many properties of these structures remain mysterious. In this study, we will analyze the growth of branched structures through a method that stresses the hierarchical structure of the branching process. This method leads to surprisingly good estimates of the fractal dimensions of diffusion-limited aggregates in various spatial dimensionalities. However, our principal interest is in the light that this approach may shed on the qualitative nature of the scaling structure, not only of diffusion-limited aggregates, but also of the more general branched structures which seem to be ubiquitous, not only in model calculations, but also in nature.

In its simplest form, diffusion-limited aggregation is a model for cluster formation in which particles arrive sequentially at a cluster surface and stick irreversibly. Before a particle strikes a cluster, it performs a random walk; particles are generally released (or created) at a large distance from the cluster, in order to simulate arrival of the particles from infinity. The $n+1$st particle is introduced into the system only after the nth particle has contacted, and stuck to, the cluster.

TABLE I. The cluster dimension D as a function of spatial dimensionality d for diffusion-limited aggregation, as obtained by numerical simulation in Ref. [3]. For $d>5$, the numerical results are not reliable.

d	D
2	1.71
3	2.49
4	3.40
5	4.33

A two-dimensional off-lattice result with 34 000 particles is displayed in Fig. 1. The highly branched nature of the cluster is immediately evident. Less obvious is the fact that the cluster is a fractal. Let us define a radius r (radius of gyration) of the cluster by

$$r^2=\sum_{i=1}^{n}(r_i-r_0)^2/n\ , \tag{1.1}$$

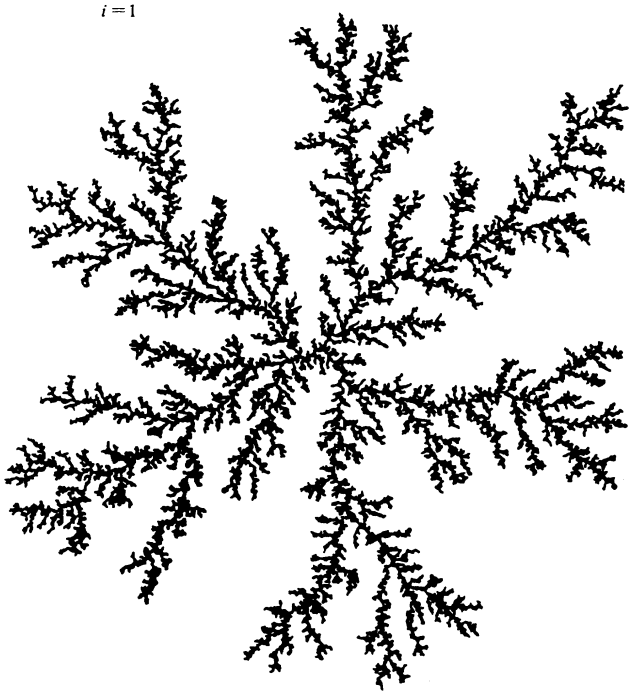

FIG. 1. A two-dimensional diffusion-limited aggregate of 34 000 particles. The structure is highly branched. In addition, it is fractal: there exist empty spaces in the structure on all length scales.

with n the number of particles, r_i the position of the ith particle, and r_0 the position of the seed particle. For particles of diameter a, one finds that $n \sim (r/a)^{D_g}$. For two-dimensional clusters, $D_g \approx 1.71$. Results for D_g in higher dimensionalities are displayed in Table I [2,3]. Since $D_g < d$, the spatial dimensionality, the asymptotic density of the clusters is zero. This is reflected in the fact that in Fig. 1, holes appear in the cluster on every length scale, the larger the cluster, the larger the proportion of the region occupied by the cluster that is covered by such holes.

Given the apparent self-similarity of the cluster in Fig. 1, a natural approach is to attempt some sort of real-space renormalization-group analysis. A number of workers have proposed such methods [4,5]; special note should be taken of the "fixed scale transformation" of Pietronero, Erzan, and Evertsz [6]. Generally these methods succeed in finding values for D_g in the two-dimensional case that are within 5% of the computational result. These methods are based on the idea that the geometry of the cluster should in some sense reflect a fixed point in the renormalization group.

Another approach has been to develop Flory type theories for the dimension based on the interaction between a random walker and a rough surface. One of the earliest such proposals was that of Muthukumar, who suggested a formula for the dimension [7]

$$D_g = \frac{d^2+1}{d+1} \ . \tag{1.2}$$

These proposals are somewhat controversial; the conservatively minded will prefer to view Eq. (1.2) as a phenomenological formula for D_g. Of course, such theories do not make any specific predictions regarding cluster structure beyond the value of D_g and possibly the multifractal dimensions (see below) [8].

Yet a third approach is based on the study of the statistical properties of the growth probability distribution. If one takes an n-particle cluster, one can define the growth probability measure on the accessible surface of that cluster, which is simply the probability that the $n+1$st particle will attach itself to the surface at any particular point. If one defines p_i as the probability that the $n+1$st particle will attach itself to the ith surface particle of the cluster, then

$$\sum_i p_i^q = \left[\frac{a}{r} \right]^{\tau(q)} \ , \tag{1.3}$$

where $\tau(q)$ is a nontrivial function of q [9]. One often works with the Legendre transform of $\tau(q)$, a function $f(\alpha)$ satisfying the following relations [10]:

$$\alpha(q) = \frac{d\tau(q)}{dq}, \quad f(q) = q\alpha(q) - \tau(q), \quad \frac{df}{d\alpha} = q \ . \tag{1.4}$$

The functions $\tau(q)$ and $f(\alpha)$ have been computed for DLA clusters by a number of groups [11–14].

Beyond their phenomenological usefulness, these functions, which encode the "multifractal" statistical properties of the growth probability distribution, satisfy certain scaling relations, which follow from the nature of diffusive growth. The first of these, proposed by Turkevich and Scher, is that [15]

$$D_g \geq 1 + \alpha_{\min} \ , \tag{1.5}$$

where $\alpha_{\min}$ is the minimum value of α appearing in the spectrum; it is easily shown from Eqs. (1.4) that $\alpha_{\min} = \lim_{q \to \infty} d\tau/dq$. [Turkevich and Scher actually proposed Eq. (1.5) as an equality.]

The growth probability measure can be shown to be proportional to the normal electric field [$P(s)$, where s indexes position on the cluster surface] at the surface of the cluster given that the cluster is at potential zero and some distant conductor is at a fixed nonzero potential. Another scaling law can be derived from the following formula for the moments of $P(s)$, which follows from elementary electrostatic considerations [16]:

$$\frac{d}{dn} \left\langle \int ds \, P(s) \right\rangle \propto \left\langle \frac{\int ds \, P^3(s)}{\int ds \, P(s)} \right\rangle \ . \tag{1.6}$$

Here the brackets $\langle \ \rangle$ refer to averaging over the ensemble of DLA clusters. If one replaces the average of a ratio on the right-hand side of this expression by a ratio of the averages, one obtains the following scaling law:

$$D_g = \tau(3) + 2 - d \ . \tag{1.7}$$

The appearance of averages of moments of the growth probability distribution over the ensemble of DLA clusters introduces the question of how this averaging might best be performed. By analogy with statistical mechanics, one can define two possible averaging procedures, quenched and annealed averaging, and their corresponding functions $\tau(q)$, by [17]

$$\tau_q(q) = -\frac{\left\langle \ln \left[\sum_i p_i^q \right] \right\rangle}{\ln(r/a)} \tag{1.8a}$$

and

$$\tau_a(q) = -\frac{\ln \left\langle \sum_i p_i^q \right\rangle}{\ln(r/a)} \ . \tag{1.8b}$$

Although in some ways $\tau_a(q)$ appears to be a more natural quantity, it is very sensitive to unusual members of the ensemble with eccentric distributions of the $\{p_i\}$ [18]. As with the statistical mechanics of systems with quenched disorder, we thus expect $\tau_q(q)$ to be more relevant for typical members of the ensemble. For small values of q, one expects $\tau_a(q) \approx \tau_q(q)$, but for larger values of q significant deviations are possible. Often one finds negative values of $f(\alpha)$ for annealed averaging (analogous to negative entropy in statistical mechanics) [19]. The scaling laws above are quite accurate for the quenched dimensions that have been computed numerically; whether they hold for the annealed dimensions is uncertain. Direct computation of the annealed dimensions, because they are sensitive to rare members of the ensemble, can only be done by exact enumeration of all DLA clusters of a particular size. This was done by Lee

and Stanley [18,20]; however, their results are for very small clusters and are probably not quantitatively reliable.

Another scaling law refers to the "information dimension" of the measure, which is $D_I = d\tau(q)/dq|_{q=1}$. Makarov has proven that for $d=2$, $D_I=1$ for probability measures proportional to the normal electric field under quite general conditions [21]. It has also been hypothesized that $D_I = d-1$ for general dimensionality [22].

For the purposes of this study, it is useful to define the multifractal dimensions in a slightly different way. We consider all clusters with a fixed number of particles n, and consider the scaling of moments of $\{p_i\}$ with n. In this way we define functions $\sigma_a(q)$ and $\sigma_q(q)$ by

$$\sigma_q(q) = -\frac{\left\langle \ln\left[\sum_i p_i^q\right]\right\rangle}{\ln n} \tag{1.9a}$$

and

$$\sigma_a(q) = -\frac{\ln\left\langle \sum_i p_i^q\right\rangle}{\ln n}\ , \tag{1.9b}$$

analogously to Eqs. (1.8a) and (1.8b). For the quenched dimensions, one expects $\sigma_q(q)=\tau_q(q)/D_0$, where $D_0 \equiv -\tau_q(0)$ is the dimension of the cluster surface. Naively, one would expect $D_0 = D_g$, but this equality is in fact a matter of some controversy. Argoul *et al.* have claimed that direct computation of the surface dimension in $d=2$ through box-counting techniques yields values of $D_0 \approx 1.60$ that are significantly less than $D_g \approx 1.71$ [23]; however, these efforts have been criticized on grounds that they incorrectly handle logarithmic corrections [24].

Of course, for the annealed dimensions the situation might be even more confusing. In this paper, we will assume the formula $\sigma_a(q)=\tau_a(q)/D_{0,a}$, with $D_{0,a}$ the annealed surface dimension. We hope that this does not introduce appreciable inaccuracies into our results.

Discussion of this somewhat bewildering menagerie of dimensions is, unfortunately, necessary for us. This is because, in our theory, we can conveniently compute only $\sigma_a(q)$, which we then wish to compare to numerical results for $\tau_q(q)$. Although, as the reader will see, the results are quite close (for small values of q), we do not know if the remaining discrepancies are due to inadequacies of our theory, or are due to differences between quenched and annealed dimensions. If DLA is analogous to other statistical systems, all such fluctuation effects are less important in higher dimensions, and we do obtain better results for $3 \le d \le 5$ than for $d=2$. For $d>5$, the literature values for D_g have rather large error bars, and we can only make qualitative judgements regarding the success of our approach.

Our model is based on two quite general features of DLA growth. As these features are observed in other types of growth as well, we believe that our approach will be useful in other growth problems. The first relevant feature of DLA growth is that it exhibits continuous tip splitting, so that local parts of the cluster consist of linear chains of particles that then split in two. Splitting of a growing tip into more than two tips is a rare process, seen only in the very early stages of growth.

The second relevant feature is that branches compete with one another for growth probability on all length scales. This process leads to the existence of dead branches, which have lost this competition, on all length scales. Furthermore, the branches compete for a diffusing field, which has no intrinsic length scale. Thus we expect that, in some sense, the dynamics of this struggle will be the same for two rather small branches competing against one another and for two quite large branches in competition.

Based on these two observations alone, we construct a general framework for hierarchical, competitive branched growth [25]. This framework has the property that for stochastic processes, it leads naturally to multifractal growth probability statistics without any further assumptions. The multifractal dimensions are calculable from an integral. For nonstochastic processes, multifractional statistics are not possible. This framework differs from the "conventional wisdom" regarding fractal growth in two respects. In the first place, the dynamics is dominated not by a stable fixed point (as in the real-space renormalization methods), but by an unstable fixed point. It is the escape of the system from this unstable fixed point at all length scales which, combined with stochasticity, leads to multifractal statistics. In the second place, the system is not self-similar in any simple way; in particular, the statistics of branch sizes in slowly growing regions of the cluster explicitly differ from these statistics in quickly growing regions of the cluster [26].

To make quantitative predictions, we must introduce a specific model of the competition dynamics of branches. It is possible to construct such models from physical arguments regarding the extent to which different branches will succeed in monopolizing a diffusing field, indeed, such a model is discussed in Appendix A. However, we prefer a more robust and less elaborate approach (model Z), in which we make the simplest possible assumption for these dynamics consistent with the principles outlined above. In Ref. [27], an alternate approach, based on screening in real and not hierarchical space, is proposed.

Using this ansatz, we self-consistently compute the dimension of DLA clusters as a function of spatial dimensionality d, assuming implicitly that $D_0 = D_g \equiv D$. We obtain $D=1.66$ for $d=2$, and $D=2.50$ for $d=3$. As $d \to 1$, we find $D \to 1$; we always have $d-1 < D \le d$, as required by exact results. As $d \to \infty$, $D \to d-1$. Values of D for various dimensions d are displayed in Table II.

TABLE II. A comparison of simulation results of the dimension D of diffusion-limited aggregates with the results of our model Z and with the Muthukumar formula, Eq. (1.2). The model Z results are within a few tenths of a percent of the Muthukumar formula over the entire range $1 \le d < \infty$.

d	$D_{\text{simulation}}$	$D_{\text{Model } Z}$	$D_{\text{Muthukumar}}$
2	1.71	1.66	1.67
3	2.49	2.50	2.50
4	3.40	3.40	3.40
5	4.33	4.33	4.33

Our results are extremely close to but are not exactly equal to the Muthukumar formula, Eq. (1.2).

It is also possible to compute the other multifractal dimensions $\tau(q)$, subject to the restrictions mentioned above. Here significant deviations are seen at large q from the simulation results; we believe this is a consequence of the difference between annealed and quenched dimensions.

We also discuss the scaling of the maximum growth probability $p_{\max}$ for typical members of the ensemble of clusters. We find that a simple mean-field type averaging procedure leads to the Turkevich-Scher hypothesis, $p_{\max} \sim n^{D^{-1}-1}$. The computation of the minimum growth probability is more difficult. No competition dynamics model will give universal values of annealed dimensions for $q<0$; this agrees with the results of Lee and Stanley [18]. The typical minimum growth probabilities, which have been the subject of some controversy [28], are dependent on details of the branch dynamics model.

Finally, it is also possible to study branch dynamics by direct numerical simulation. This we have done, and we have found qualitative agreement with the picture proposed above. However, certain features of the realistic branch dynamics are not reflected in our theoretical model; this model must thus be viewed as an idealization of the true situation, though one that seems qualitatively and even quantitatively adequate.

This paper is organized into six sections and four appendixes. Section II introduces the hierarchical framework, and shows how stochasticity leads naturally to multifractal statistics. Section III addresses the construction of specific competition dynamics models, and introduces and solves model Z. We compute multifractal exponents for this model and compare them with previous work. Section IV addresses the estimation of the minimum and maximum growth probabilities for a typical cluster. In Sec. V, we show how competition dynamics can be extracted from numerical data, and discuss similarities and differences between these results and the idealized picture of Secs. II and III. Section VI concludes and discusses shortcomings of the theory. In Appendix A, we discuss a different competition dynamics model (model A) which, though not quantitatively adequate, has some interesting features. In Appendix B, we discuss nonstochastic models, and discuss why these models can show power-law behavior of growth probabilities without possessing multifractal statistics. In Appendix C, we discuss the mathematical reasons for the close agreement between the Muthukumar formula Eq. (1.2) and the results of model Z. In Appendix D, we present an alternative computation of the multifractal partition function.

II. THE HIERARCHICAL MODEL

The possibility of constructing a binary hierarchical model for branched growth follows from two simple empirical observations. Each particle that arrives at a DLA cluster has a well-defined parent, the particle to which it sticks. Thus one can define a genealogical tree of particles, leading back to the original seed particle (see Fig. 2) [25]. Almost all particles have asymptotically either one or two children; particles with more than two children are seen only at the very top of the hierarchy, near the seed particle. Furthermore, almost all of the growth takes place at the bottom of the hierarchical tree, downstream from the last "node," or particle with more than one child. Our numerical results (see Sec. V below) show that for large two-dimensional clusters 92% of the growth probability is downstream from the last node in the hierarchical tree, and 97% is downstream from the second to the last node. Not only is DLA growth dominated by an active zone when seen in real space, but it is also dominated by an active zone in this genealogical space.

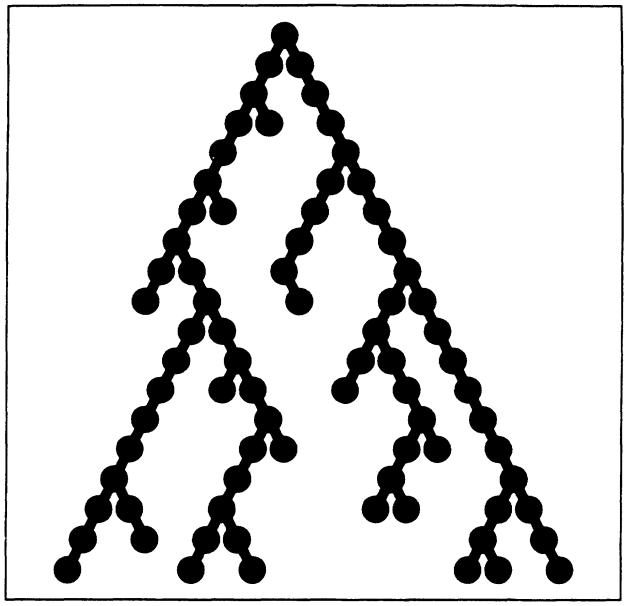

FIG. 2. Since each particle in off-lattice diffusion-limited aggregation attaches itself to a unique parent, one can construct a genealogical tree corresponding to, e.g., the aggregate of Fig. 1. Except near the top of the tree, close to the seed particle, each particle has either one or two descendants.

We will assume a binary hierarchy, in which growth takes place entirely in the last level of the hierarchy. We will further assume that the growth process is such that the competition between two siblings (branches emanating from the same node) at any level in the hierarchy is determined by their relative masses and probabilities, but not by the structure of the cluster exterior to these two siblings, nor by their own internal structure.

We thus seek to describe two sibling branches by their masses n_1 and n_2 and by their total growth probabilities p_1 and p_2. We use $n_b = n_1 + n_2$ to describe the entire mass of the two siblings taken together. These quantities are perfectly well defined for any dynamics; we introduce an assumption in saying that their change as the cluster grows is affected only by one another. We introduce two normalized quantities,

$$x = \frac{p_1}{p_1 + p_2} \tag{2.1}$$

and

$$y=\frac{n_1}{n_1+n_2} . \tag{2.2}$$

We immediately obtain an equation of motion for y from the definition of p_1 as a growth probability,

$$\frac{dy}{d\ln n_b}=\frac{dn_1}{dn_b}-\frac{n_1}{n_b}=x-y . \tag{2.3}$$

This is generally valid. The quantitative form of our assumption about competition is that we can write a similar equation for x,

$$\frac{dx}{d\ln n_b}=g(x,y) , \tag{2.4}$$

where g is not a function of any other variable describing structure. Clearly we expect by symmetry that $g(x,y)=-g(1-x,1-y)$.

There are three obvious fixed points of these dynamics. At $(x,y)=(\frac{1}{2},\frac{1}{2})$, symmetry implies that $g(x,y)=0$, and $dy/d\ln n_b=0$. This corresponds to the case where both branches have equal mass and equal growth probability. We expect that $(x,y)=(0,0)$ and $(x,y)=(1,1)$ will also be fixed points of the dynamics, as in these cases one branch has all the mass and all the growth probability. This implies that $g(0,0)=g(1,1)=0$.

If the fixed point at $(x,y)=(\frac{1}{2},\frac{1}{2})$ is stable, then the other fixed points must be unstable, and vice versa. If the former case holds, all sibling branches, no matter how unequally they are created, will always asymptotically approach a state in which the two siblings are perfectly equal in both mass and growth probability. This is probably the case in some branched growth processes, notably for the "dense branched morphology" [29]. On the other hand, if the fixed point at $(x,y)=(\frac{1}{2},\frac{1}{2})$ is unstable, then we expect that asymptotically at most one sibling of any pair will remain active, while the other will be perfectly dead. This is characteristic of diffusion-limited aggregation.

An unstable fixed point may have two unstable directions; one unstable direction and one marginal direction (in which case it lies on a fixed line), or one unstable direction and one stable direction. The reader will see in Sec. V that the numerical evidence suggests the second of these possibilities for DLA; here we shall concentrate on the latter possibility (actually, we believe that the first possibility leads to a very similar theory, but we will not consider it further in this study.)

Now if the fixed point at $(x,y)=(\frac{1}{2},\frac{1}{2})$ is hyperbolic, with one unstable and one stable direction, then most of the trajectories of branch competition will lie rather close to the unstable manifold of the fixed point (see Fig. 3). This is particularly the case for trajectories that start quite close to the fixed point; we shall see below that these trajectories dominate in determining the asymptotic scaling properties of the system. We are thus led to the following simplified model. Consider the unstable manifold of the fixed point at $(x,y)=(\frac{1}{2},\frac{1}{2})$. We regard pairs of sibling branches as starting out on this manifold at the value $n_b\sim 1$ at some distance from the unstable fixed point. As they mature, and acquire more particles, they move along the unstable manifold, ending as $n_b\to\infty$ in one of the two stable fixed points for which one of the branches has entirely won the competition. Of course, the entire pair could die at finite n_b to competition on yet longer length scales, in which case the relative probabilities and masses of the two siblings will remain fixed at some intermediate values for the remaining history of the growth process.

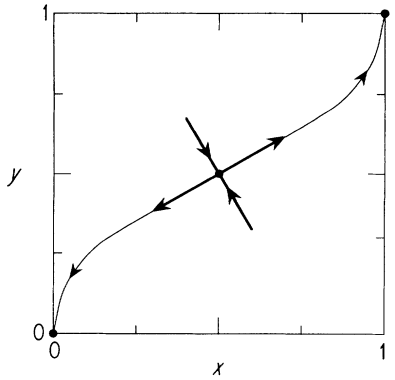

FIG. 3. This diagram exhibits an approximation to the competition dynamics of two sibling branches. The x axis measures the relative growth probabilities of the two branches, $x=p_1/(p_1+p_2)$, and the y axis measures the relative masses of the two branches, $y=n_1/(n_1+n_2)$. The development of these two quantities as functions of $n_b=n_1+n_2$ can be represented in this diagram. The fixed point at the center represents equal branches, the two fixed points at the corners represent branch pairs in which one branch completely dominates the other. At the central fixed point, we suppose that there is one stable and one unstable eigenvector.

It is useful to make a preliminary analysis of the dynamics near the unstable fixed point. Suppose that

$$\left.\frac{\partial g(x,y)}{\partial x}\right|_{(1/2,1/2)}=g_x \tag{2.5}$$

and

$$\left.\frac{\partial g(x,y)}{\partial y}\right|_{(1/2,1/2)}=g_y . \tag{2.6}$$

Then the product of the two eigenvalues is $-(g_x+g_y)$, which we are assuming to be negative. Suppose the eigenvector in the unstable direction has the form

$$\vec{\lambda}=\begin{bmatrix} c \\ 1 \end{bmatrix} . \tag{2.7}$$

Then we know that the corresponding eigenvalue is $\nu=c-1$, because we know the second row of the stability matrix at the fixed point from Eq. (2.3).

A second preliminary is related to the initial distribution of the distance of branch pairs from the unstable fixed point. From the equations of motion for (x,y), we

see that near the fixed point we expect

$$x=\tfrac{1}{2}-k_0 n_b^{\nu} \tag{2.8a}$$

and

$$y=\frac{1}{2}-\frac{k_0 n_b^{\nu}}{c}\ , \tag{2.8b}$$

where $|k_0|$ is proportional to the initial distance of the branch pair (when $n_b=1$) from the fixed point. Instead of k_0, we use ϵ as our random parameter, and find it convenient to define

$$x=\tfrac{1}{2}-(\epsilon n_b)^{\nu} \tag{2.9a}$$

and

$$y=\frac{1}{2}-\frac{(\epsilon n_b)^{\nu}}{c}\ . \tag{2.9b}$$

If we assume that the probability distribution of branch starting positions $\rho(\epsilon)$ is uniform in the x-y plane near the unstable fixed point, then we need $\lim_{\epsilon\to 0}\rho(\epsilon)=\rho_0\epsilon^{\nu-1}$, with ρ_0 some constant. The distribution function $\rho(\epsilon)$ is really determined by the microscopic processes which nucleate branches; the assumption that we have just made can be strictly justified only by a detailed theory of these processes. It is difficult to see, however, how such a theory could lead to singular behavior near $(x,y)=(\frac{1}{2},\frac{1}{2})$ at a microscopic level. Thus, although we will write $\lim_{\epsilon\to 0}\rho(\epsilon)=\rho_0\epsilon^{\tilde{\nu}-1}$, we actually believe that $\tilde{\nu}=\nu$.

A final preliminary is related to this exponent $\tilde{\nu}$. Suppose that asymptotically during the branch competition process, we reach a situation in which not only does $y\to 0$ (or $y\to 1$), but it goes to zero at least as fast as $1/n_b$. This is a feature of all of the specific models that we shall propose for DLA, and implies that the disfavored branch dies completely, so that it asymptotes to a final mass n_f which no longer changes as the other sibling continues to grow. In this case, it is easy to see that due to the way in which ϵ and n_b combine in Eqs. (2.3), (2.4), (2.9a), and (2.9b), we have

$$\lim_{n_b\to\infty} y(\epsilon n_b)=\frac{n_f}{n_b}=\frac{y_0}{\epsilon n_b}\ , \tag{2.10}$$

so that $n_f=y_0/\epsilon$, where $y_0\sim 1$ is a constant depending on details of the trajectory. Thus the distribution of sizes of dead branches is related to the distribution of ϵ, and thus to $\tilde{\nu}$.

Now consider a growing cluster, in which we regard the main genealogical line as corresponding to the path down the binary tree that always chooses the stronger sibling. If this path is directed outwards from the seed particle in a more or less straight line, as is the case for DLA, then the total number of sidebranches off of this path is $\sim r$, because the sidebranches are separated by a microscopic distance. But the largest sidebranch should have a number of particles of the order of n, as otherwise there would be no dead branches of a size of the order of magnitude of the cluster size, and the entire cluster would be made up of the active, growing zone, which contradicts the assumption that most branches are dead (as well as numerous observations of DLA [2,3]. Actually, the converse of this implies that $n\sim r$, or $D_g=1$. The probability $P(n)$ that a particular sidebranch is of size n is

$$P(n)\sim\int_0^{y_0/n} d\epsilon\,\rho(\epsilon)\sim n^{-\tilde{\nu}}\ , \tag{2.11}$$

so the probability $P_{\rm tot}(n)$ that one of the $\sim r$ sidebranches has this size is

$$P_{\rm tot}(n)\sim n^{-\tilde{\nu}} r\ , \tag{2.12}$$

which is ~ 1 by the argument above. Thus we conclude that $\tilde{\nu}=1/D_g$, where D_g is the radius of gyration exponent discussed in Sec. I above.

Now we are in a position to relate the trajectory of Fig. 3 to the multifractal spectrum of the growth probabilities for the associated growth process. For a particular branch, we can write

$$x(n_b,\epsilon)=x(\eta\equiv\epsilon n_b),\quad y(n_b,\epsilon)=y(\eta\equiv\epsilon n_b)\ . \tag{2.13}$$

Given the unstable manifold $y(x)$, we can construct the functions $x(\eta)$ and $y(\eta)$ from an integration of Eq. (2.3).

We will compute $\sigma_a(q)$ using the partition function approach [10]. In this approach, we consider all branches below the last node, on which we are assuming all growth probability to lie. Indexing these branches by j, we define $Z(q,\sigma)$ by

$$Z(q,\sigma)=n^{\sigma}\sum_j \frac{p_j^q}{n_j^{\sigma}}\ , \tag{2.14}$$

with p_j the total probability of the jth branch, n_j its mass, and n the total number of particles in the cluster. Now we expect that $\sigma(q)$ may be defined implicitly by the condition

$$\lim_{n\to\infty} Z(q,\sigma)=1\ , \tag{2.15}$$

as is customary for multifractal systems.

Consider a hierarchical tree as in Fig. 4. We will assume that all mass and probability of a branch on a large length scale can be unambiguously attributed to its constituent sub-branches (although this is difficult for segments of particles close to the seed). It is a trivial matter to deal with this omission, and we shall henceforth ignore it. We will now compute the contribution of the partition function of two sibling branches at the bottom of the tree. We suppose that the path from the top of the tree passes first through a node for which the value of ϵ is ϵ_0, then through a node for which the value of ϵ is ϵ_1, and so forth down to the node for which springs the two siblings that concern us, for which the value of ϵ will be ϵ_N. For notational convenience, we also assume that we always choose the path at every node corresponding to the weakest branch (except at the end, when we include the contributions of both of the two sibling branches). Then the contribution of the two branches A and B at the bottom of

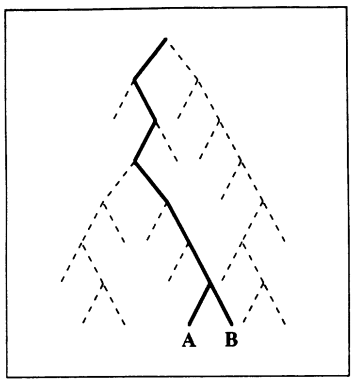

FIG. 4. Two branches A and B at the bottom of the hierarchical tree.

the tree to the partition function is

$$Z(q,\sigma)_{A,B}=\frac{x^q(\epsilon_0 n)}{y^\sigma(\epsilon_0 n)}\frac{x^q(\epsilon_1 n_1)}{y^\sigma(\epsilon_1 n_1)}\cdots \times\left\{\frac{x^q(\epsilon_N n_N)}{y^\sigma(\epsilon_N n_N)}+\frac{[1-x(\epsilon_N n_N)]^q}{[1-y(\epsilon_N n_N)]^\sigma}\right\}, \tag{2.16}$$

where $n_1=ny(\epsilon_0 n)$ is the mass of the entire weaker branch at the top of the tree; similarly, n_N is the mass of the branches A and B taken together. This mass depends on all values of ϵ along the path that was taken to the bottom of the tree. Thus averaging $Z(q,\sigma)_{A,B}$ over $\{\epsilon\}$ is not necessarily an easy task. Note that we have taken $x<\frac{1}{2}$.

We will start by performing the average over ϵ_N. This particular random variable appears only in the term in braces in Eq. (2.16), so the (annealed) average that we need to perform is

$$z_{A,B}=\int d\epsilon_N \rho(\epsilon_n)\left\{\frac{x^q(\epsilon_N n_N)}{y^\sigma(\epsilon_N n_N)}+\frac{[1-x(\epsilon_N n_N)]^q}{[1-y(\epsilon_N n_N)]^\sigma}\right\}, \tag{2.17}$$

which has a nontrivial dependence on n_N, and thus on all of the other random variables. Since $\int d\epsilon\rho(\epsilon)=1$, we can rewrite this as

$$z_{A,B}=1+\int d\epsilon_N \rho(\epsilon_N)\left\{\frac{x^q(\epsilon_N n_N)}{y^\sigma(\epsilon_N n_N)}+\frac{[1-x(\epsilon_N n_N)]^q}{[1-y(\epsilon_N n_N)]^\sigma}-1\right\}. \tag{2.18}$$

Although this seems like a trivial charge, it is crucial to the successful computation of $\sigma_a(q)$. The quantity in braces $\{\}$ now goes to zero for large values of $\epsilon_N n_N$. Suppose that n_N is large (i.e., that we stopped this decomposition into branches well above the microscopic scale). Then the integral will be dominated by its behavior for small values of ϵ_N, provided that the quantity in braces goes to zero faster than $\epsilon_N^{-\tilde{\nu}}$ at large ϵ_N. If we assume this to be the case (this proves to be true for all physical models that we have examined; it is also in agreement with our numerical results), then we can replace $\rho(\epsilon_N)$ by its small ϵ_N form given above. Substituting $\eta=\epsilon_N n_N$, we then obtain

$$z_{A,B}=1+\frac{\rho_0}{n_N^{\tilde{\nu}}}\int d\eta\,\eta^{\tilde{\nu}-1}\left\{\frac{x^q(\eta)}{y^\sigma(\eta)}+\frac{[1-x(\eta)]^q}{[1-y(\eta)]^\sigma}-1\right\}, \tag{2.19}$$

so that all of the effect of the other random variables is included in a simple factor multiplying the integral. It is now elementary to show that a necessary and sufficient condition for $\langle Z(q,\sigma)\rangle=1$ is that $z_{A,B}=1$, because in this case one can simply repeat the decomposition that we have performed here by integrating over ϵ_{N-1} (which also influences the "first cousins" of A and B), etc. In Appendix D, we present an alternative calculation of the partition function, which implies that the corrections to Eq. (2.19) do not asymptotically affect the partition function.

Thus we arrive at our equation relating the trajectory followed by two competing branches to $\sigma_a(q)$,

$$\int_0^\infty d\eta\,\eta^{\tilde{\nu}-1}\left\{\frac{x^q(\eta)}{y^\sigma(\eta)}+\frac{[1-x(\eta)]^q}{[1-y(\eta)]^\sigma}-1\right\}=0\,. \tag{2.20}$$

This holds provided that the quantity in braces $\{\}$ is bounded as $\eta\to\infty$ by a power law $\eta^{-\gamma}$, with $\gamma>\tilde{\nu}$. If branch death occurs, then $\gamma=1$; furthermore, for the small η portion of the integral to converge, we need $\tilde{\nu}>0$. Thus we conclude that we must have $0<\tilde{\nu}<1$ for this integral criterion to be meaningful. Note that this tallies nicely will our claim above that for branched growth in which branch death occurs, $\tilde{\nu}=1/D_g$. Obviously, $D_g<1$ is impossible for branched growth.

III. A SPECIFIC CASE: MODEL Z

In this section, we will introduce a family of specific models for the trajectory $y(x)$, and compute the corresponding multifractal spectra $\sigma_a(q)$. We can fix the dimension by using the result from Sec. I regarding the information dimension, which implies that $\tilde{\nu}(d-1)=[d\sigma_a(q)/dq]|_{q=1}$. The model that we shall propose possesses one free parameter; by varying this parameter while requiring this equality we can obtain a self-consistent result for $D(d)$, and also for other multifractal dimensions as a function of d, subject to the assumptions regarding averaging discussed in Sec. I above.

This model, which we call model Z, is based on the observation that near the unstable fixed point, we expect $y(x)$ to be a linear trajectory $y-\frac{1}{2}=(x-\frac{1}{2})/c$ following the most unstable eigenvector at that fixed point. For large values of $|x-\frac{1}{2}|$ and $|y-\frac{1}{2}|$, the trajectory should curve down into the stable fixed point at $(x,y)=(0,0)$. A reflected trajectory goes into the other stable fixed point at $(x,y)=(1,1)$. In model Z we assume that the linear behavior round the unstable fixed point persists as long as possible, i.e., until $x=0$ (or $1-x=0$) and one of the

branches has completely won the competition for growth probability. At this point, the branch that has won continues to grow, while the other remains with a fixed number of particles and no growth probability. In the x-y diagram, this corresponds to a vertical trajectory into the fixed point (see Fig. 5).

We are assuming, for reasons discussed in Sec. II above, that if the slope of the trajectory near the fixed point is $1/c$, then $\tilde{\nu}=c-1$. Thus fixing the value of c determines all properties of the model. Furthermore, $0<\tilde{\nu}<1$ implies that $1<c<2$, so that the trajectory leaving the fixed point must pass between the dashed lines in Fig. 5.

Model Z is equivalent to assuming that the form of the function $g(x,y)$, which determines the redistribution of growth probability between the competing branches, can be approximated everywhere in the x-y plane by its form near the unstable fixed point, which is given by Eqs. (2.5) and (2.6). Obviously, we can give no physical justification of this, nor do we expect it to be exactly true. The virtue of model Z is that it is simple, and that it is only a one-parameter model, which allows us to make a robust quantitative comparison between its results and simulation results on DLA. In Sec. V below, the reader will see that the actual trajectories followed by competing branches have considerable qualitative similarity to those assumed by model Z. In Appendix A, we discuss a more elaborate, physically motivated model.

The integral, Eq. (2.20), will now be given by two terms corresponding to the two portions of the model Z trajectory. The first portion leads from the unstable fixed point to the boundary line $x=0$. Writing $\delta=\eta^{\tilde{\nu}}$, we can write this portion of the integral as

$$I_1(q,\sigma,c)=\frac{1}{c-1}\int_0^{1/2}d\delta\left[\frac{(1/2-\delta)^q}{(1/2-\delta/c)^\sigma}+\frac{(1/2+\delta)^q}{(1/2+\delta/c)^\sigma}-1\right]. \tag{3.1}$$

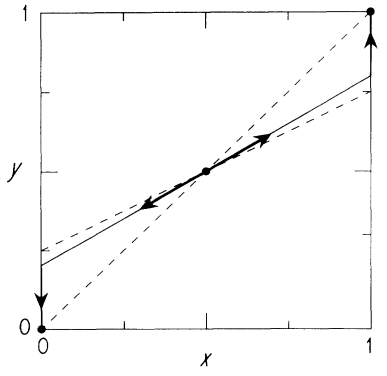

FIG. 5. In model Z, we suppose that branch competition follows the trajectory indicated. First the branches follow a continuation of the unstable eigenvector at the fixed point. After one branch has lost all growth probability, the branches follow vertical trajectories into one of the stable fixed points. The unstable eigenvector must lie between the dashed lines.

The other part of the trajectory contributes to term $I_2(\sigma,c)$, which is given by

$$I_2(\sigma,c)=\int_{\eta_f}^{\infty}d\eta\,\eta^{\tilde{\nu}-1}\left[\frac{1}{[1-(\eta'/\eta)]^\sigma}-1\right], \tag{3.2}$$

with $\eta_f^{\tilde{\nu}}=\frac{1}{2}$, and $\eta'/n_f=(c-1)/2c$.

We determine $\sigma_a(q)$ by requiring that $I_1(q,\sigma_a(q),c)+I_2(\sigma_a(q),c)=0$, which determines $\sigma_a(q)$ as a functional of c, and thus of $\tilde{\nu}=c-1$. We then fix $c(d)$, or $\tilde{\nu}(d)$, by requiring that $\sigma'(q)|_{q=1}=(d-1)\tilde{\nu}$. Lengthy but straightforward algebraic manipulations of Eqs. (3.1) and (3.2) then give the following relation between $\tilde{\nu}=D^{-1}$ and d:

$$\frac{1}{d-1}=\tilde{\nu}G(\tilde{\nu}), \tag{3.3}$$

and

$$G(\tilde{\nu})=1-\tilde{\nu}-\left[\frac{\tilde{\nu}^2}{2}\right]\ln\left[\frac{\tilde{\nu}}{2+\tilde{\nu}}\right]+2\sum_{n=1}^{\infty}\frac{1}{(n-\tilde{\nu})}\left[\frac{\tilde{\nu}}{2(1+\tilde{\nu})}\right]^n. \tag{3.4}$$

This equation is easily solved numerically to give $D(d)$. Results are displayed as a continuous function of d in Fig. 6; Table II shows numerical results for various low dimensionalities. As $d\to\infty$, $D\to d-1$, and as $d\to 1$, $D\to 1$. Furthermore, $d-1<D\le d$ always. As noted in Table II, the Muthukumar formula $D=(d^2+1)/(d+1)$ gives a highly accurate approximation to these results over the entire range of d; however, the Muthukumar formula is not exactly the same as the model Z results. We discuss the mathematical reason for the close correspondence between the model Z results and the Muthukumar formula in Appendix C.

For fixed d, one can also compute the multifractal spectrum $\sigma_a(q)$ or $\tau_a(q)=D\sigma_a(q)$. Results for $d=2$ are shown in Fig. 7 and are tabulated in Table III. The

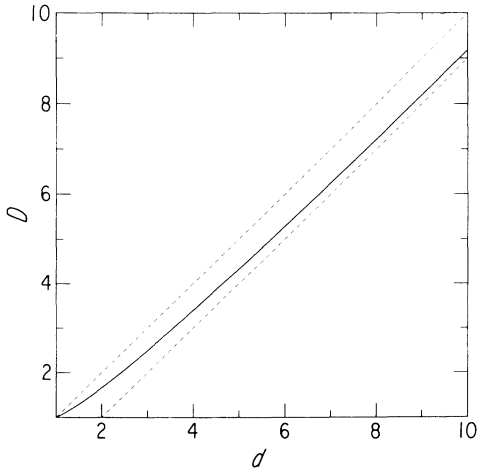

FIG. 6. Model Z leads to the illustrated cluster dimension D as a function of spatial dimensionality d. D always satisfies $d-1<D\le d$. The cases $D=d-1$ and d are indicated by dashed lines.

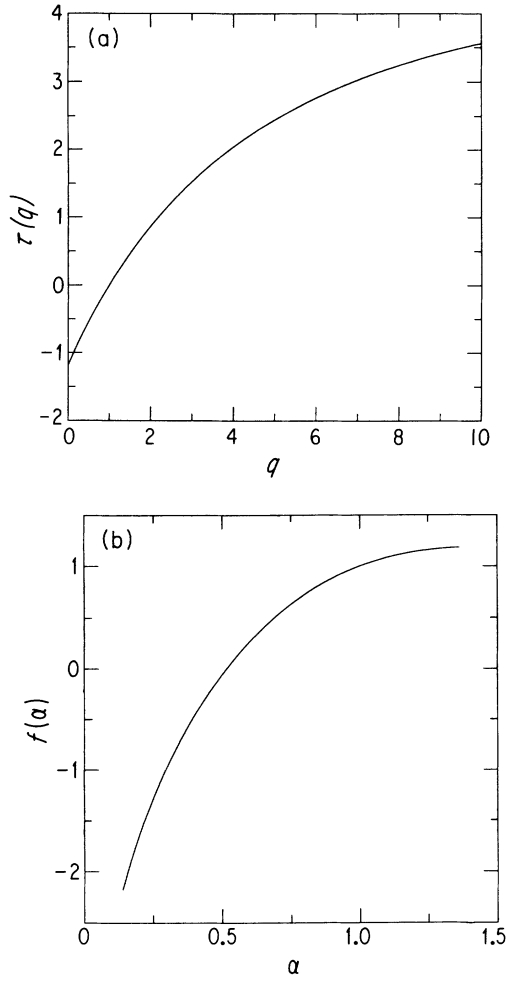

FIG. 7. (a) The annealed multifractal spectrum $\tau(q)$ for model Z in two dimensions. The fact that $\lim_{q\to 0}\tau(q)\neq D$ is an artifact of model Z. (b) The annealed multifractal spectrum $f(\alpha)$ for model Z in two dimensions. At small α, $f(\alpha)$ becomes negative.

reader will note that at large values of q, negative values of $f(\alpha)$ are obtained, as is typical for annealed averages [19,20]. Furthermore, the value of $\tau_a(3)$ is significantly different from D, suggesting that the electrostatic scaling law may not hold for annealed averages. Finally, for $q<0$, model Z gives no answers for $\tau_a(q)$; these dimensions are unlikely to exist for real DLA either.

As $q\to 0_+$, model Z is unrealistic because the growth probabilities of the weaker siblings have been set to zero exactly over part of the trajectory. This is a good approximation to the real case, in which these probabilities are extremely small (see Sec. V below), but gives an incorrect result for $\lim_{q\to 0_+}\sigma_a(q)$.

TABLE III. Model Z values of the annealed multifractal dimensions $\tau(q)$ or $f(\alpha)$ for various values of q and the corresponding values of α. For large q, or small α, we find negative $f(\alpha)$.

q	$\tau(q)$	$\alpha(q)$	$f(\alpha)$
1	0.00	1.00	1.00
2	0.87	0.75	0.64
3	1.53	0.58	0.21
4	2.04	0.45	−0.23
5	2.47	0.36	−0.66

IV. MAXIMUM AND MINIMUM GROWTH PROBABILITIES

As we remarked in the Introduction, annealed averages for $\sigma(q)$, although relatively early to perform, are not necessarily very relevant for typical members of the ensemble of clusters, particularly at large values of q. In this section, we will present simple arguments regarding the scaling behavior of the maximum and minimum growth probabilities, $p_{\max}$ and $p_{\min}$. These arguments are specifically designed to be appropriate for typical members of the ensemble. Our result for the scaling of $p_{\max}$ is, in fact, identical to a scaling law proposed by Turkevich and Scher, which we reviewed in the Introduction. Thus our approach is at least superficially consistent with the result of Turkevich and Scher.

The maximum growth probability of all sites in the cluster is obtained by going down the binary tree, choosing always the branch with the largest growth probability. Thus we can write

$$\ln(p_{\max})=\sum_i \ln[1-x(\epsilon_i n_i)]\ , \tag{4.1}$$

where ϵ_i and n_i are, respectively, the random parameter and the mass at the ith branching, as in Sec. II above.

Our procedure will be to average $x(\epsilon_i n_i)$ over ϵ_i, thus obtaining an average loss of growth probability to the sidebranch at the ith branching. We will then use this averaged x to obtain the average loss of mass.

In particular,

$$\int d\epsilon_i \epsilon_i^{\tilde{\nu}-1} x(\epsilon_i n_i)=\frac{x_0}{n_i^{\tilde{\nu}}}\ , \tag{4.2}$$

where x_0 is a constant of order one. Since this quantity is typically small, we write

$$\langle \ln(p_{\max})\rangle \approx -\sum_i \frac{x_0}{n_i^{\tilde{\nu}}}\ . \tag{4.3}$$

To perform the sum, we must have at least an approximate form for n_i. But we can compute $\langle dn_i/di\rangle$ from Eq. (4.2),

$$\left\langle \frac{dn_i}{di}\right\rangle = -\int^{n_i} dn(x)=\frac{x_0}{(\tilde{\nu}-1)n_i^{\tilde{\nu}-1}}\ , \tag{4.4}$$

so that we obtain

$$\langle \ln(p_{\max})\rangle \approx -\sum_i \frac{x_0}{n_i^{\tilde{\nu}}} \approx \int^n dn\left\langle \frac{dn}{di}\right\rangle^{-1}\frac{x_0}{n^{\tilde{\nu}}}$$
$$=(\tilde{\nu}-1)\ln n\ . \tag{4.5}$$

Using $\tilde{\nu}=1/D$, this reduces to the Turkevich-Scher relation

$$\ln(p_{\max})=\left[\frac{1}{D}-1\right]\ln n \ . \tag{4.6}$$

Or, since $n \propto r^D$, and $\ln(p_{\max})=-\alpha_{\min}\ln r$,

$$D=1+\alpha_{\min} \ . \tag{4.7}$$

Note that we have made no assumptions about the origin of the growth probability measure in this argument, so we expect this result to hold for a larger class of models than DLA models alone. The reader will observe that our averaging procedure has a mean-field flavor; this may account for deviations from the Turkevich-Scher law seen in numerical computations of $\alpha_{\max}$ [13,14].

Now we turn to the minimum growth probability $p_{\min}$. In the above discussion of $p_{\max}$, the exact nature of the trajectory in the x-y plane, or equivalently the function $g(x,y)=dx/d\ln n_b$, did not figure. However, although we believe that the maximum value of the growth probability is not sensitive to details of the function $g(x,y)$, we believe that the minimum value of the growth probability is quite sensitive to its form near $(x,y)=(0,0)$ [or equivalently near $(x,y)=(1,1)$].

We expect on physical grounds that a branch, once dead, does not resurrect itself. This implies that $g(0,y)=0$. In a physically motivated, model A, discussed in Appendix A, $g(x,y)$ has the following form for small x,y:

$$g(x,y)\approx -kx \ , \tag{4.8}$$

with k a constant.

Now let us suppose that the lowest probability region of the cluster corresponds to the disfavored branch at the first branching in the hierarchy. Since typically $\epsilon\sim 1$, we expect the total number of particles in this branch to be ~ 1. Furthermore, it is the most completely screened dead branch. The growth probability of this branch $p_{\min}$ is then easily computed from

$$\frac{dp_{\min}}{d\ln n}=-kp_{\min} \ , \tag{4.9}$$

yielding

$$p_{\min}\propto n^{-k} \ , \tag{4.10}$$

in agreement with multifractal statistics.

Schwarzer *et al.* have claimed that $p_{\min}$ actually scales in a qualitatively different way with n [28],

$$\ln(p_{\min})\propto(\ln n)^{\beta} \ , \tag{4.11}$$

with $\beta\approx 2$. It is easy to show that this corresponds to the following behavior of $g(x,y)$ for x,y small:

$$g(x,y)\propto x[\ln(x)]^{1-1/\beta} \ . \tag{4.12}$$

Thus if Schwarzer *et al.* are correct, we expect a logarithmic singularity in $g(x,y)$. This implies a trajectory steeper than any power law near $(x,y)=(0,0)$, which is consistent with the claim that model Z is a good approximation to the trajectory.

V. NUMERICAL RESULTS

In this section, we present results of a numerical study of branch competition. We use these results to determine an averaged trajectory in the x-y plane, and thereby directly compute annealed dimensions for DLA (within the hierarchical model). We find reasonable qualitative agreement with the discussion of Secs. II and III; the annealed dimension that we compute, $D\approx 1.6$, is considerably lower than the radius of gyration exponent of a typical cluster.

To measure growth probabilities and branch sizes for a cluster we must first create a DLA. Efficient algorithms for diffusion-limited aggregation are described elsewhere [2,3,30]. In using these algorithms, it is important to record not only the position of each particle that joins the cluster, but also the identity of each particle's parent, the particle to which it sticks. In order to insure that each particle has a unique parent, all of our clusters are grown off lattice.

Next, we determine the growth probability for each particle in the cluster. This can be done by relaxing the diffusion equation with the cluster as a boundary. We use the method of simultaneous overrelaxation to solve this problem [31]. (This method proved to be unstable in the deepest fjords of the DLA, and we follow the overrelaxation with several iterations of simple relaxation in order to get accurate results.) Unfortunately, this numerical method requires the use of a lattice, and thus we project our off-lattice clusters onto a square lattice. As a result, we actually measure the probability for growth at a particular lattice site, and not the probability for a diffusing particle to attach itself to a particular particle. In cases where several particles are adjacent to a growth site, we divide the growth probability equally between the neighboring particles. From these growth probabilities, we directly find that 92% of the total growth probability is downstream from the last node of the cluster, and 97% is downstream from the second to the last node, as mentioned in Sec. II.

There are two possible methods of studying branch competition. In the first, we create a cluster with $n(1)$ particles. We then relax the diffusion equation onto the cluster and determine the values of (x,y) for all pairs of sibling branches. We then continue the growth process for the same cluster up to a larger size $n(2)$. For this cluster, we determine the values of (x,y) for all branch pairs appearing in the cluster. In this way we can directly measure the evolution of those branches that were present in the smaller cluster. We repeat this procedure up to a cluster of size $n(m)$. The extent to which the growth trajectories for different branches follow a single path indicates how well the branched growth is described by the hierarchical model. Because in this approach we follow the development of each branch sequentially through the growth process, we call this the sequential time picture.

In a second method, we consider all of the branch pairs in a single DLA of n particles. From each pair, we obtain one set of values for (x,y) which, according to the hierarchical model, completely describes the state of

growth for that branch pair. If we assume that in a large DLA there will be branch pairs at every stage of development, then a plot of (x,y) for all pairs should illustrate the complete branch development trajectory. The advantage of this method is that it is possible to grow many DLA's of the same size, and each of these clusters should have the same statistical distribution of branch pairs in each stage of development. Thus we can average over many realizations of the DLA cluster to get a more accurate description of the proper evolution trajectory. We will refer to this as the equal time picture.

We can make use of either of these approaches to find a trajectory that describes the branch development in DLA clusters. Once this trajectory is known, we then integrate Eq. (2.3), $dy/d\ln n_b = x - y$, to determine the functional dependence of x and y on $\ln n_b$. We can then numerically integrate Eq. (2.20), thus determining the annealed multifractal spectrum. The exponent $\tilde{\nu} = 1/D$ is determined self-consistently from the slope of the multifractal spectrum at $q = 1$.

A. Sequential time results

The data presented in this section are derived from 5 DLA clusters whose branch structure and growth probabilities were first measured at $n(1) = 2000$ and then again every 1000 particles up to $n(9) = 10\,000$. In order to keep the plots uncluttered with the inherently noisy data that describe the earliest stages of branch pair growth, we plot only those branch pairs which satisfy the following conditions: (i) each individual branch has at least four particles, and (ii) the total number of particles in a branch pair is greater than 100. Typical results are shown in Fig. 8.

Not all of these sequential trajectories lie on a common path. Thus the hierarchical model does not completely describe the branching structure of DLA. However, the trajectories rarely cross one another, thus the supposition that there exists a function $g(x,y)$ that determines branch competition appears, from these data, to be reasonable. Note that many of the branch pairs which find themselves near the line $y = x$ do not evolve away from their initial state. These points represent branch pairs which have been created in a place in which there is very little subsequent growth, so that neither branch comes to dominate the other. This behavior always occurs close to the line $x = y$, and is well described by the model of Appendix A.

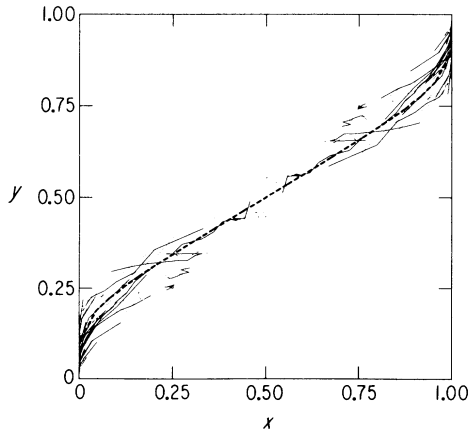

FIG. 8. Branch competition trajectories from the sequential time picture. These results show the competition of the branches of two DLA clusters whose branch structure and growth probabilities were measured at $n = 2000, 3000, \ldots, 10\,000$. The branches almost always flow away from the central point. The dashed line is the two-parameter curve that best fits all of the sequential time data set.

We shall attempt to find a single trajectory that represents an average over these results. We are thus fitting dispersed trajectories into the Procrustean bed of a single trajectory, in order to be able to apply the hierarchical model. This picture ignores the effects of correlations between different branch pairs, as well as in the fact that many trajectories seem to originate not near $(x,y) = (\frac{1}{2},\frac{1}{2})$, but elsewhere on a fixed line $x = y$.

To determine this single trajectory, we perform a least-squares fit to the branch pair data. To implement the least-squares method, we must choose a functional form for our trajectory. We choose to fit to

$$y = \begin{cases} [(2x)^{w_0}/2]\left[1 + \sum_{i=1}^{M} w_i (x - \frac{1}{2})^i\right], & x \le \frac{1}{2} \\ 1 - y(1-x), & x > \frac{1}{2}, \end{cases} \tag{5.1}$$

where the value of M for a curve indicates the number of terms in the series used to fit the data. The two properties that recommend this form are that is passes through the three fixed points at (0,0), $(\frac{1}{2},\frac{1}{2})$, and (1,1) and that $dy/dx \to \infty$ as $(x,y) \to (0,0)$ or $(x,y) \to (1,1)$. The slope at $x = \frac{1}{2}$ is given by $dy/dx|_{1/2} = w_0 + w_1/2$ for all values of M.

The fitting procedure begins by choosing a set of $\{w_i\}$. We then calculate the minimum distance between each point in the data set and the fitted curve. We choose the $\{w_i\}$ which minimizes the sum of these distances squared. We eliminate the worst outliers by first fitting to the complete set of data, and then removing all data that are beyond a fixed distance from this initial fitting curve. The values quoted for the parameters $\{w_i\}$ are the best fit to this reduced data set.

We find that taking $M = 1$ yields the best results (for $M > 1$ unphysical oscillations appear). The resulting best fit parameters are

$$w_0 = 0.22 \pm 0.01, \quad w_1 = 0.8 \pm 0.1, \tag{5.2}$$

where the error bars are subjective. From the slope of this curve at $x = \frac{1}{2}$, we can obtain a value for the exponent ν,

$$\nu = 0.61 \pm 0.17. \tag{5.3}$$

With this functional form for the branch development trajectory, we can calculate the multifractal spectrum in the hierarchical model. For each curve, we integrate the equation

$$\eta \frac{dy}{d\eta} = x(\eta) - y(\eta) \tag{5.4}$$

to determine the functional dependence of x and y on η.

Once the branch evolution trajectory is known as a function of η, we numerically integrate

$$I=\int_0^\infty d\eta\,\eta^{\tilde{\nu}}\left[\frac{x^q(\eta)}{y^\sigma(\eta)}+\frac{[1-x(\eta)]^q}{[1-y(\eta)]^\sigma}-1\right] \tag{5.5}$$

for fixed values of q and σ. The function $\sigma_a(q)$ is defined as the value of σ which causes this integral to vanish for a fixed value of q. This function is the annealed multifractal spectrum for DLA.

We fix the exponent $\tilde{\nu}$ by requiring it to be equal to the value of the slope of $\sigma_a(q)$ at $q=1$ (both of these should be equal to $1/D$). Using this self-consistent method, we find the value

$$\tilde{\nu}=0.61\pm0.01\ . \tag{5.6}$$

Note that this value of $\tilde{\nu}$ is within the (large) error bars quoted for ν. The annealed dimension predicted is $D=1.64\pm0.03$. We can also compute the annealed multifractal spectrum, shown in Fig. 9.

We are also interested in the behavior of the evolution trajectory near $(x,y)=(0,0)$ or $(1,1)$. The behavior of the curve near this point determines the scaling of $p_{\min}$, as discussed in Sec. IV. Figure 10 shows $\log_{10}(y)$ vs $\log_{10}(x)$ for the sequential time trajectories. Although the data is quite disperse, each trajectory has an approximate power-law behavior as $x\to0$. It is this steep approach to the fixed point which is responsible for the success of model Z. The trajectories also exhibit some nonpower law curvature, which may evince logarithmic corrections corresponding to the Schwarzer *et al.* scaling form (4.12) for $p_{\min}$.

B. Equal time results

In Fig. 11, we display values of (x,y) for 50 DLA clusters of size $n=3000$. We have removed all of the branch pairs with a total size $n_b<50$, as well as branch pairs in which either one of the branches contained less than four particles.

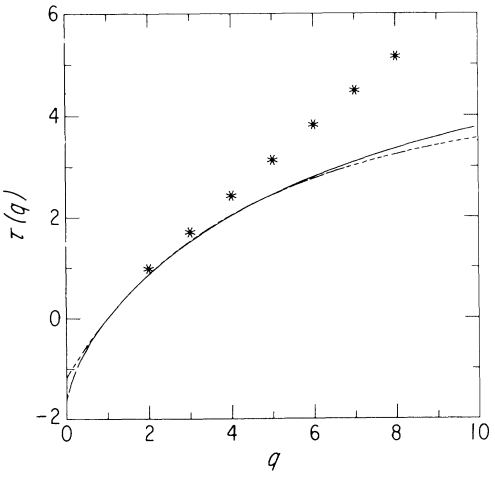

FIG. 9. Multifractal spectra for DLA. The solid line shows the annealed spectrum measured by our numerical studies of the branch growth trajectories for the sequential time picture. The equal time picture gives almost identical results. The dashed line shows the annealed spectrum predicted by model Z. The stars are the numerical results for the quenched dimensions, from Ref. [11].

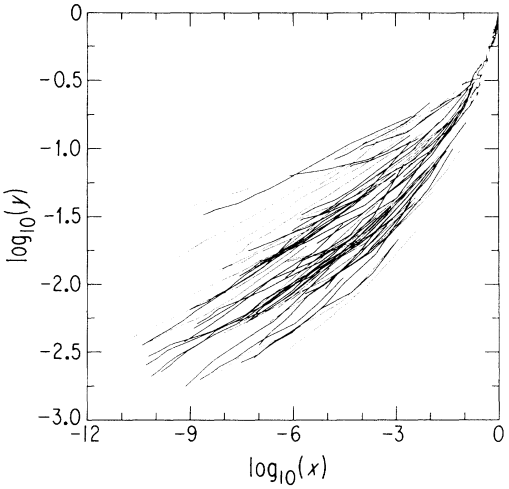

FIG. 10. Logarithmic plot of the small x behavior of the branch pair evolution trajectories. The data shown are identical to those shown in Fig. 8. Note that although each curve has almost linear behavior, the data show some curvature.

Clearly these data do not define a single trajectory. However, we can make the same assumption as above and consider these data as scatter about a single trajectory. This is not completely unreasonable; for instance, 76% of the points fall into the relatively narrow range between the two dashed lines. We are again interested in finding the best-fit curve through the data, and we again fit to the functional form Eq. (5.1) with $M=1$. The results of the fitting procedure are shown graphically in Fig. 11. The values for the best-fit parameters are

$$w_0=0.28\pm0.02,\quad w_1=0.68\pm0.08\ . \tag{5.7}$$

We use these numbers to calculate the slope at $x=\frac{1}{2}$, and

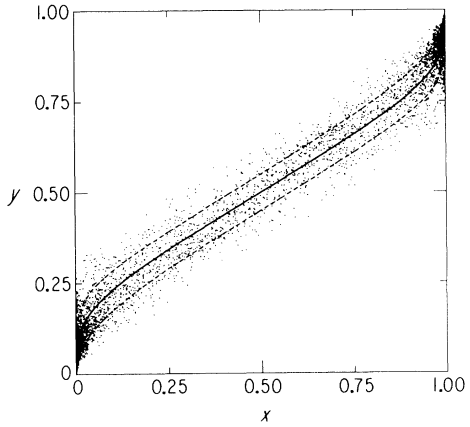

FIG. 11. The branch pair data for the equal time picture. These data were taken from 50 DLA clusters with $n=3000$. The solid line is the best-fit curve using our two parameter fit. 76% of the data lie between the two dashed lines.

thus predict the exponent

$$\nu = 0.67 \pm 0.15 \ . \tag{5.8}$$

Applying the same self-consistency condition that was used in the sequential time picture, we determine the exponent $\tilde{\nu}$ and the annealed multifractal spectrum from this data. We find

$$\tilde{\nu} = 0.62 \pm 0.02 \ , \tag{5.9}$$

so that we obtain $D = 1.61 \pm 0.05$, in agreement with our results from the sequential time picture. The annealed multifractal spectrum that results from the constant time data differs by only 3% from that computed with the sequential time data.

Finally, we can calculate directly the function $\rho(\epsilon)$ if we assign a value of ϵ to each point of the branch pair data. We do this by first finding the point P on the evolution trajectory which is closest to the point P' of the branch data set. We then calculate the value of η for P and assign that value of η to P'. Once η is known for a given branch pair, we use the relation $\eta = \epsilon n_b$ to find the value of ϵ. Following this procedure for every point in the data set, we can determine the probability density $\rho(\epsilon)$. The results of this calculation for DLA are shown in Fig. 12. In the power-law regime, we obtain the exponent

$$\tilde{\nu} = 0.54 \pm 0.10 \ , \tag{5.10}$$

in agreement with the self-consistent computations of $\tilde{\nu}$.

VI. DISCUSSION

Although on a phenomenological level, the theory described above is quite successful, there are a number of difficulties with this approach on a more fundamental level. The numerical evidence is in reasonably good agreement with the proposition that the function $g(x,y)$ exists, as shown by the infrequency with which trajectories cross one another in the x-y plane. However, the integral formalism that we have introduced can be justified in the way in which we have done so only if the unstable fixed point is hyperbolic, so that there is a well-defined unstable manifold. Both the numerical evidence, and the analysis of a physically motivated model (model A) in Appendix A, suggest that there is a fixed line in the x-y plane, the line $x = y$; this fixed line is unstable in the direction orthogonal to itself. Thus the unstable manifold theory of this study must be generalized to account for trajectories leaving the unstable line along its entire length, or else a reason must be given for why only one of these trajectories dominates the partition function.

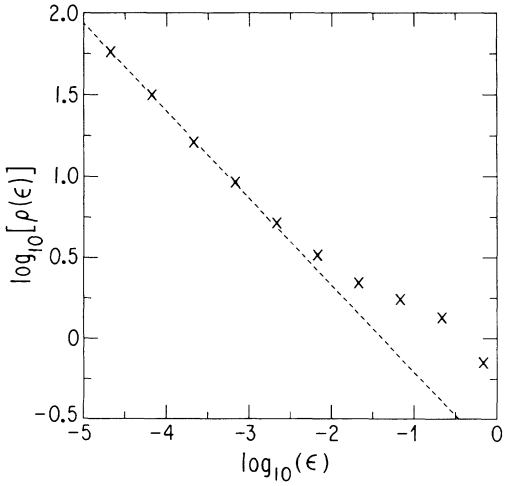

FIG. 12. Logarithmic plot of $\rho(\epsilon)$ vs ϵ for DLA. The procedure used is described in the text. The dashed line corresponds to $\tilde{\nu} = 0.54$. This power-law behavior of $\rho(\epsilon)$ agrees with our model for branched growth.

A further problem arises in considering the function $g(x,y)$. In principle, the competition of two branches depends on the behavior of the rest of the cluster, as well as on the internal structure of the two branches. Thus, in principle, g depends not only on the parameters describing the relative masses and growth probabilities of the branches being considered, but also on these parameters for all other branch pairs in the system. In restricting our attention to x and y for the competing branch pair alone, we are making an assumption about the irrelevance of these other parameters, which we have not quantitatively justified.

A related problem relates to the specific structure of $g(x,y)$. We have made a fortuitous choice for this function in model Z; the accuracy of the resultant dimensions suggest that this choice may become exact, at least in the neighborhood of the unstable manifold, in some limit. A complete theory of DLA would include a computation of $g(x,y)$ from first principles. It would be interesting to see if the real-space methods developed by Pietronero and others can be used to compute $g(x,y)$ [4–6].

Finally, a serious technical lacuna in our treatment of model Z is our failure to compute quenched as well as annealed dimensions for this model. The computation of quenched dimensions in the general case for stochastic multifractal systems is a difficult and as yet unsolved problem; perhaps this work will stimulate more interest in this area.

Note added in proof. In collaboration with K. Honda, we have computed quenched dimensions for model Z [37]. The results for $D(d)$ are almost exactly the same as those reported in Sec. III above. For large values of q, the quenched dimensions for model Z are much closer to numerical results for DLA than are the annealed dimensions calculated in Sec. III.

ACKNOWLEDGMENTS

We would like to acknowledge stimulating discussions with R. Goldstein, K. Honda, L. P. Kadanoff, and T. A. Witten. T.C.H. is very grateful to A. Libchaber for encouragement at an early stage in this project. We are also grateful to A. Chhabra for assistance with the numerical work reported in Sec. V. We thank P. Ossadnik for bringing Ref. [3] to our attention, and J. Lee for providing unpublished results. This work was supported by the Materials Research Laboratory of the University of Chicago and by the National Science Foundation, Grant No. DMR-9057156.

APPENDIX A: ALTERNATIVE MODELS OF BRANCH COMPETITION

In this appendix we will derive a one-parameter family of physical models (model A) for the competition of two

branches. These models are not especially realistic—they yield trajectories in the x-y plane that are significantly different from those found in Sec. V; furthermore, they give quantitatively inadequate values for the dimensions of diffusion-limited aggregates. Nevertheless, we believe that, as an exercise, the development of this model is informative. Some features of this model, particularly the appearance of a fixed line, are reminiscent of the numerical results discussed in Sec. V.

We commence by considering two DLA branches in isolation. We presume that each branch can be viewed as a circle as regards its ability to absorb probability flux; we further choose the two circles corresponding to the two branches to be in contact. Thus our first task is to compute the relative probabilities that a random walker arriving from ∞ will strike one of two circles in contact, with radii r_1 and r_2.

In general, two circles may be mapped onto two concentric circles by a Möbius transformation [32]. We determine this transformation first for two circles not in contact, and then we take the limit in which the circles touch. We place the center of the first circle (circle C_1 of radius r_1) at (0,0) and the center of the second circle (circle C_2 of radius r_2) at (1,0). First we must find the circle C' that intersects both of these circles at right angles—the Möbius transformation that maps this circle onto the imaginary axis maps C_1 and C_2 onto concentric circles.

The cross ratio of four complex numbers (z_1,z_2,z_3,z_4) is invariant under a Möbius transformation. Thus if the transformation maps the complex u plane to the complex v plane, then

$$\frac{(u_1-u_2)(u_3-u)}{(u_1-u_3)(u_2-u)}=\frac{(v_1-v_2)(v_3-v)}{(v_1-v_3)(v_2-v)} . \tag{A1}$$

Suppose that the center of C' is at $(\gamma',0)$, and that its radius is λ. A straightforward calculation using Eq. (A1) yields

$$\gamma'=\tfrac{1}{2}(1+r_1^2-r_2^2) \tag{A2}$$

and

$$\lambda=[\tfrac{1}{4}(1+r_1^2-r_2^2)^2-r_1^2]^{1/2} . \tag{A3}$$

Having determined γ' and λ, we can now proceed to find the appropriate transformation that takes our system onto two concentric circles. We know that we want $(\gamma'-\lambda,0)\to(0,0)$, $(\gamma'+\lambda,0)\to\infty$, and $(r_1,0)\to(1,0)$. This is sufficient to determine the transformation. Take $v_1=(0,0)$, $v_2=(1,0)$, and $v_3=\infty$. Then

$$v=\frac{[(\gamma'-\lambda)-u\,](\gamma'+\lambda-r_1)}{[(\gamma'+\lambda)-u\,](\gamma'-\lambda-r_1)} . \tag{A4}$$

Let us define $\gamma=(\gamma'+\lambda)/r_1$, $\gamma^{-1}=(\gamma'-\lambda)/r_1$, and $\tilde{u}=u/r_1$. Then we may rewrite v as

$$v=\frac{(1-\gamma\tilde{u})(1-\gamma^{-1})}{(1-\gamma^{-1}\tilde{u})(1-\gamma)}=\frac{(\gamma\tilde{u}-1)}{(\gamma-\tilde{u})} . \tag{A5}$$

Two quantities of particular interest are the radius of the image of the point at ∞, $v_\infty\equiv v(u\to\infty)$, and the radius of the outer concentric circle, $v_{\rm out}\equiv v[u=(1-r_2,0)]$, which are, respectively, given by

$$v_\infty=\gamma \tag{A6}$$

and

$$v_{\rm out}=\frac{\{\gamma[(1-r_2)/r_1]-1\}}{\gamma-[(1-r_2)/r_1)]} . \tag{A7}$$

From elementary electrostatics and the properties of conformal transformations we know that the probabilities of a random walker striking the two circles are $p_1\propto\ln(v_\infty)$ and $p_2\propto\ln(v_{\rm out}/v_\infty)$. Thus by taking the limits of the expressions above as $r_1+r_2\to1$ we can obtain p_1 and p_2.

More specifically, write $r_1+r_2=1-\varepsilon$. Some simple algebra yields

$$v_{\rm out}=1+\frac{\sqrt{2\varepsilon}}{\sqrt{r_1r_2}}+O(\varepsilon) \tag{A8}$$

and

$$v_\infty=\gamma=1+\sqrt{2\varepsilon}\sqrt{r_2/r_1}+O(\varepsilon) . \tag{A9}$$

Now we can directly calculate the relevant logarithms,

$$\ln(v_{\rm out}/v_\infty)=\sqrt{2\varepsilon/r_1r_2}(1-r_2)\approx\sqrt{2\varepsilon}\sqrt{r_1/r_2} \tag{A10}$$

and

$$\ln(v_\infty)=\sqrt{2\varepsilon}\sqrt{r_2/r_1} . \tag{A11}$$

Thus we obtain the final result,

$$p_1=\frac{r_1}{r_1+r_2} , \tag{A12}$$

$$p_2=\frac{r_2}{r_1+r_2} , \tag{A13}$$

so that the relative growth probabilities of the two circles are determined by their relative radii.

Now suppose that $dr_1/dn_1=(r_1/Dn_1)$, where D is the cluster dimension. It follows directly that

$$\frac{dp_1}{d\ln n}=-\frac{dp_2}{d\ln n}=kp_1p_2\left[\frac{p_1}{n_1}-\frac{p_2}{n_2}\right] , \tag{A14}$$

with $k=D^{-1}$. This equation, combined with Eq. (2.3) for $dn_1/d\ln n_b$, gives a complete description of trajectories in the x-y plane. It is simple to rewrite this equation in terms of the variables x,y of Sec. II,

$$\frac{dx}{d\ln n_b}=kx(1-x)\left[\frac{x}{y}-\frac{1-x}{1-y}\right] , \tag{A15}$$

and, of course,

$$\frac{dy}{d\ln n_b}=x-y . \tag{A16}$$

Although we have derived Eqs. (A15) and (A16) for a specific two-dimensional model, we shall now regard them as a description of branch competition in the x-y plane on all length scales as functions of x and y.

These equations possess a marginal line $x=y$ (a prop-

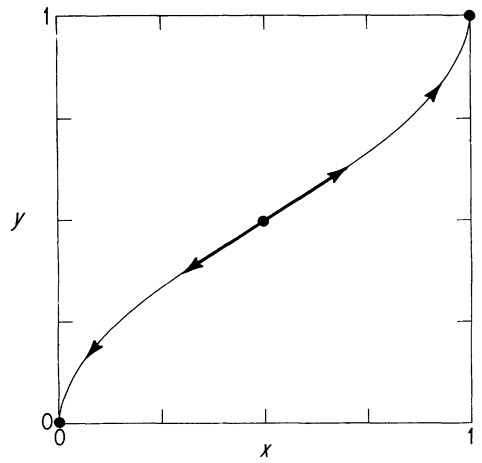

FIG. 13. The trajectory of branch competition in model A for $k=1.6$. The trajectory is more curved than either model Z or the numerical trajectories of Sec. V.

erty in agreement with the numerical results of Sec. V). However, for $k<1$, this line is stable. This should not surprise us unduly, as an instability of this "two-branch" model would conflict with the direct stability analysis of Ball for clusters with various numbers of macroscopic branches [33]. However, if we generalize this model by assuming that

$$p_1=\frac{r_1^{\zeta}}{r_1^{\zeta}+r_2^{\zeta}}=1-p_2 , \tag{A17}$$

then a simple computation yields Eq. (A15) with $k=\zeta/D$. A typical trajectory, for $k=1.6$, is shown in Fig. 13. If we now consider general spatial dimensionality, then by varying k, we obtain a one-parameter family of models, whose corresponding $D(d)$ can be computed following the method of Sec. II. We assume in an *ad hoc* manner that the dominant trajectories start at $(x,y)=(\frac{1}{2},\frac{1}{2})$. Results are shown in Table IV; although $D(d\to\infty)\to d-1$, the numerical values of this dimension are not satisfactory by comparison to DLA. This is not surprising, as the trajectory of Fig. 13 looks nothing like the trajectories seen for branch competition in our numerical studies reported in Sec. V.

TABLE IV. A comparison of simulation values of the dimension D with those computed from model A for various spatial dimensionalities d. The model A values are not close to those computed by simulation, although the model A results do have $\lim_{d\to\infty}D=d-1$.

d	D_{DLA}	$D_{\mathrm{Model\ A}}$
2	1.71	1.50
3	2.49	2.28
4	3.40	3.18
5	4.33	4.06

APPENDIX B: NONSTOCHASTIC MODELS

To study nonstochastic branched growth, we need only generalize the theory developed in Sec. II to the case where the $\{\epsilon\}$ are a constant for all branches. We can fix this constant to be $\epsilon=1$ by a redefinition of the trajectory function $(x(n),y(n))$. If we write the partition function of a branch of n particles as $\Gamma(n,q,\sigma)$, we obtain

$$\Gamma(n,q,\sigma)=\frac{x^q(n)}{y^{\sigma}(n)}\Gamma(y(n)n,q,\sigma)+\frac{[1-x(n)]^q}{[1-y(n)]^{\sigma}}\Gamma([1-y(n)]n,q,\sigma) . \tag{B1}$$

Now we wish to fix $\sigma(q)$ by requiring $\Gamma(n,\sigma,q)=1$. The limiting function obtained as $n\to\infty$ will then be the asymptotic $\sigma(q)$. In general, we expect the right-hand side of Eq. (B1) to be dominated by one or the other of its two terms as $n\to\infty$. If the first term dominates, then we expect

$$\sigma(q)=q\lim_{n\to\infty}\frac{\ln[x(n)]}{\ln[y(n)]} , \tag{B2}$$

while if the second term dominates, then we expect

$$\sigma(q)=q\lim_{n\to\infty}\frac{\ln[1-x(n)]}{\ln[1-y(n)]} . \tag{B3}$$

Although we can use these results to compute maximum and minimum growth probabilities, there is no general multifractal (i.e., not piecewise linear) solution $\sigma(q)$. As an example, consider the case $x(n)=x_0n^{-\gamma}$. A simple computation yields $y(x)=x_0n^{-\gamma}/(1-\gamma)$, provided $\gamma<1$. If the second term in Eq. (B1) dominates, then from Eq. (B3) we obtain

$$\sigma=q(1-\gamma) , \tag{B4}$$

so that the maximum probability scales with n as $p_{\max}\propto n^{\gamma-1}$. Since the Turkevich-Scher law should apply to this system, this implies $D=\gamma^{-1}$. If we suppose that the first term dominates, then from Eq. (B2) we obtain

$$\sigma=q . \tag{B5}$$

This result yields $p_{\min}\propto n^{-1}$. Thus we do not expect nonstochastic branched growth to contain any strongly screened growth sites, except those arising from interbranch interactions not treated in the hierarchical model.

Suppose that we are considering nonstochastic diffusive growth. If the growth measure is different from the normal electric field at the surface by small quantities only, then we expect that the electrostatic scaling law will apply to this model. [Note that the same conclusion does not necessarily apply to the Makarov law, as the information dimension is inherently more sensitive to small changes in the growth probabilities than is $\tau(3)$.] If we can apply Eq. (B4) away from $q\to\infty$, then using the scaling law Eq. (1.7),

$$\sigma(3)=1+\frac{d-2}{D} , \tag{B6}$$

combined with $D=1/\gamma$, we obtain $D=(d+1)/2$. This conclusion agrees with the well-established result that

$D=\frac{3}{2}$ in $d=2$ for noise-reduced diffusion-limited aggregation [34]. For $d>3$, it violates the "causality bound" $D\geq d-1$ [35]. This suggests that the noise-reduced branched fixed point may not exist in high dimensions.

APPENDIX C: MODEL Z AND THE MUTHUKUMAR FORMULA

In Sec. III, we observed that the dimensions computed from model Z via Eqs. (3.3) and (3.4) are quite close (within a few tenths of a percent) to the Muthukumar formula $D=(d^2+1)/(d+1)$. This approximate equality has a rather peculiar mathematical origin, which we shall explain in this appendix.

We start by reviewing our formula for the dimension $D=\tilde{\nu}^{-1}$ as an implicit function of d,

$$\frac{1}{d-1}=\tilde{\nu}G(\tilde{\nu})\ . \tag{C1}$$

The function $G(\tilde{\nu})$ is given by

$$G(\tilde{\nu})=1-\tilde{\nu}-\frac{\tilde{\nu}^2}{2}\ln\left[\frac{\tilde{\nu}}{2+\tilde{\nu}}\right] +2\sum_{n=1}^{\infty}\frac{1}{n-\tilde{\nu}}\left[\frac{\tilde{\nu}}{2(1+\tilde{\nu})}\right]^n . \tag{C2}$$

$G(\tilde{\nu})$ has simple poles at the positive integers $G(\tilde{\nu}=1,2,3,\ldots)$ and a weak logarithmic singularity at $\tilde{\nu}=0$. (The apparent logarithmic singularity at $\tilde{\nu}=-2$ is actually cancelled by a contribution from the sum.)

Now $\lim_{\tilde{\nu}\to 0}G(\tilde{\nu})=1$, which implies that $\lim_{d\to\infty}D=d-1$. Because of the logarithmic singularity at $\tilde{\nu}=0$, a power-series expansion about this result is not possible. As $\tilde{\nu}\to 1$, $G(\tilde{\nu})$ can be written as

$$G(\tilde{\nu})=a_{-1}(1-\tilde{\nu})^{-1}+a_0+a_1(1-\tilde{\nu})+O((1-\tilde{\nu})^2)\ , \tag{C3}$$

with $a_{-1}=0.5$, $a_0=0.4431$, and $a_1=-0.1794$.

Now to understand the accuracy of the Muthukumar formula, we observe that it has the form of a Padé approximant. If we consider approximations to D by ratios of quadratic to linear polynomials in $(d-1)$,

$$D\approx\frac{b_0+b_1(d-1)+b_2(d-1)^2}{1+c_1(d-1)}\ , \tag{C4}$$

then the only form consistent with $\lim_{d\to\infty}D=d-1$, $D(d=1)=1$, and $a_{-1}=0.5$ is the Muthukumar formula

$$D=\frac{d^2+1}{d+1}\ . \tag{C5}$$

Instead of using information from both $d\to\infty$ and 1 to constrain the Padé approximant, we can directly compute the (2,1) Padé approximant corresponding to the expansion Eq. (C3) about $d=1$ [36]. After some tedious computation, we obtain the result

$$D\approx\frac{e_0+e_1(d-1)+e_2(d-1)^2}{1+f_1(d-1)}\ . \tag{C6}$$

TABLE V. Values of the Padé coefficients from Eq. (C6) for model Z compared to the Muthukumar formula values of these coefficients.

	Model Z	Muthukumar
e_0	1	1
e_1	0.7593	1
e_2	0.3512	$\frac{1}{2}$
f_1	0.2593	$\frac{1}{2}$

In Table V, we compare these values of the Padé coefficients, obtained by expansion about $d=1$, to the Muthukumar values of these coefficients. Only at $O(d-1)^3$ are there significant deviations between (C5) and (C6).

APPENDIX D: COMPUTING THE PARTITION FUNCTION

In this appendix, we will more carefully justify the integral criterion for $\sigma_a(q)$ introduced in Sec. II. We start by writing a general relation for the partition function as an integral equation, which follows from the hierarchical assumption,

$$\mathcal{Z}(q,\sigma,n)=\int_0^{\infty}d\epsilon\,\rho(\epsilon)\left[\frac{x^q(\epsilon n)}{y^{\sigma}(\epsilon n)}\mathcal{Z}[q,\sigma,y(\epsilon n)n] +\frac{[1-x(\epsilon n)]^q}{[1-y(\epsilon n)]^{\sigma}} \times\mathcal{Z}(q,\sigma,[1-y(\epsilon n)]n)\right] . \tag{D1}$$

This can be written in more compact form if we define $x(-\epsilon n)=1-x(\epsilon n)$, $y(-\epsilon n)=1-y(\epsilon n)$, and $\rho(-\epsilon)=\rho(\epsilon)$, in which case Eq. (D1) can be written as

$$\mathcal{Z}(q,\sigma,n)=\int_{-\infty}^{\infty}d\epsilon\,\rho(\epsilon)\frac{[1-x(\epsilon n)]^q}{[1-y(\epsilon n)]^{\sigma}} \times\mathcal{Z}(q,\sigma,[1-y(\epsilon n)]n)\ . \tag{D2}$$

If we assume that the integral is dominated by values of $[1-y(\epsilon n)]n\approx n$, then we can expand the integrand,

$$\mathcal{Z}(q,\sigma,n)=\int_{-\infty}^{\infty}d\epsilon\,\rho(\epsilon)\frac{[1-x(\epsilon n)]^q}{[1-y(\epsilon n)]^{\sigma}}\mathcal{Z}(q,\sigma,n) -n\int_{-\infty}^{\infty}d\epsilon\,\rho(\epsilon)y(\epsilon n)\frac{[1-x(\epsilon n)]^q}{[1-y(\epsilon n)]^{\sigma}} \times\frac{d\mathcal{Z}(q,\sigma,n)}{dn}+O\left[\frac{d^2\mathcal{Z}}{dn^2}\right] . \tag{D3}$$

Let us write

$$\int_{-\infty}^{\infty}d\epsilon\,\rho(\epsilon)\frac{[1-x(\epsilon n)]^q}{[1-y(\epsilon n)]^{\sigma}}=1+\frac{g_0}{n^{\tilde{\nu}}}+\cdots\ , \tag{D4}$$

where the higher-order terms vanish more quickly with n than $n^{-\bar{\nu}}$. We also write

$$\int_{-\infty}^{\infty} d\epsilon \rho(\epsilon) y(\epsilon n) \frac{[1-x(\epsilon n)]^q}{[1-y(\epsilon n)]^\sigma} = \frac{h_0}{n^{\bar{\nu}}} + \cdots , \quad \text{(D5)}$$

since $\lim_{\epsilon \to \infty} y(\epsilon n) = 0$. Again, the higher-order terms vanish more quickly with n than $n^{-\bar{\nu}}$. Thus we obtain

$$\frac{d \ln Z}{d \ln n} \approx \frac{g_0}{h_0} , \quad \text{(D6)}$$

so that we must have $g_0 = 0$ in order that the partition function not diverge, or go to zero, as $n \to \infty$. This is the same criterion as that we used in Sec. II, i.e., that the part of the integral Eq. (D4) proportional to $n^{-\bar{\nu}}$ should vanish. It is easy to see from Eq. (D3) that the terms higher order in n^{-1} in the integral do not prevent $\lim_{n \to \infty} Z \to 1$. Naively, one would expect that the corrections to Eq. (D5) should go as n^{-1}, implying that as $\bar{\nu} \to 1$, corrections to the integral result may become troublesome. This is a conceivable explanation for the numerical difficulties in two dimensions that are reflected in the controversy between Ref. [23] and [24].

[1] T. A. Witten, Jr. and J. M. Sander, Phys. Rev. Lett. **47**, 1400 (1981).

[2] P. Meakin, Phys. Rev. A **27**, 1495 (1983).

[3] S. Tolman and P. Meakin, Phys. Rev. A **40**, 428 (1989).

[4] H. Gould, F. Family, and H. E. Stanley, Phys. Rev. Lett. **50**, 686 (1983); T. Nagatani, Phys. Rev. A **36**, 5812 (1987); J. Phys. A **20**, L381 (1987); P. Barker and R. C. Ball, Phys. Rev. A **42**, 6289 (1990).

[5] X. R. Wang, Y. Shapir, and M. Rubenstein, Phys. Rev. A **39**, 5974 (1989); J. Phys. A **22**, L507 (1989).

[6] L. Pietronero, A. Erzan, and C. Evertsz, Phys. Rev. Lett. **61**, 861 (1988); Physica A **151**, 207 (1988).

[7] M. Muthukumar, Phys. Rev. Lett. **50**, 839 (1983).

[8] M. Matsushita, Y. Hayakawa, S. Sato, and K. Honda, Phys. Rev. Lett. **59**, 86 (1987).

[9] A. Renyi, *Probability Theory* (North-Holland, Amsterdam, 1970); B. B. Mandelbrot, Ann. Phys. Soc. (Israel) **2**, 225 (1977); H. G. E. Hentschel and I. Procaccia, Physica D **8**, 435 (1983).

[10] T. C. Halsey, M. H. Jensen, L. P. Kadanoff, I. Procaccia, and B. Shraiman, Phys. Rev. A **33**, 1141 (1986); U. Frisch and G. Parisi, in *Turbulence and Predictability in Geophysical Fluid Dynamics and Climate Dynamics,* Proceedings of the International School of Physics "Enrico Fermi" Course LXXXVIII, Varenna, 1984, edited by M. Ghil, R. Benzi, and G. Parisi (North-Holland, Amsterdam, 1985), p. 84.

[11] T. C. Halsey, P. Meakin, and I. Procaccia, Phys. Rev. Lett. **56**, 854 (1986). For a recent experimental study, see F. Mas and F. Sagués, Europhys. Lett. **17**, 541 (1992).

[12] P. Meakin, H. E. Stanley, A. Coniglio, and T. A. Witten, Jr., Phys. Rev. A **32**, 2364 (1985).

[13] C. Amitrano, A. Coniglio, and F. di Liberto, Phys. Rev. Lett. **57**, 1016 (1986); C. Amitrano, Phys. Rev. A **39**, 6618 (1989).

[14] Y. Hayakawa, S. Sato, and M. Matsushita, Phys. Rev. A **36**, 1963 (1987).

[15] L. Turkevich and H. Scher, Phys. Rev. Lett. **55**, 1026 (1985); Phys. Rev. A **33**, 786 (1986).

[16] T. C. Halsey, Phys. Rev. Lett. **59**, 2067 (1987); Phys. Rev. A **38**, 4749 (1988).

[17] M. E. Cates and T. A. Witten, Phys. Rev. A **35**, 1809 (1987); T. C. Halsey, in *Fractals: Physical Origin and Properties,* edited by L. Pietronero (Plenum, London, 1989).

[18] J. Lee and H. E. Stanley, Phys. Rev. Lett. **61**, 2945 (1988).

[19] B. B. Mandelbrot, J. Stat. Phys. **34**, 895 (1984); A. B. Chhabra and K. R. Sreenivasan, Phys. Rev. A **43**, 1114 (1991).

[20] J. Lee and H. E. Stanley (unpublished).

[21] N. G. Makarov, Proc. London Math. Soc. **51**, 369 (1985).

[22] P. Jones (unpublished).

[23] F. Argoul, A. Arneodo, G. Grasseau, and H. L. Swinney, Phys. Rev. Lett. **61**, 2558 (1988).

[24] G. Li, L. M. Sander, and P. Meakin, Phys. Rev. Lett. **63**, 1322 (C) (1989); R. C. Ball and O. Rath Spivack, J. Phys. A **23**, 5295 (1990).

[25] A number of groups have recently studied the hierarchical structure of DLA clusters. We note in particular B. Derrida, V. Hakim, and J. Vannimenus, Phys. Rev. A **43**, 888 (1991); P. Ossadnik, *ibid.* **45**, 1058 (1992).

[26] There is considerable qualitative evidence that the scaling structure of the low-growth-probability regions of DLA differs from that of the high-growth-probability regions. See, e.g., B. Mandelbrot and C. J. G. Evertsz, Nature (London) **348**, 143 (1990).

[27] R. C. Ball and M. Blunt, Phys. Rev. A **39**, 3591 (1989).

[28] R. Blumenfeld and A. Aharony, Phys. Rev. Lett. **62**, 2977 (1989); R. C. Ball and R. Blumenfeld, Phys. Rev. A **44**, 828 (1991); S. Schwarzer, J. Lee, A. Bunde, S. Havlin, H. E. Roman, and H. E. Stanley, *ibid.* **65**, 603 (1990); S. Schwarzer, J. Lee, S. Havlin, H. E. Stanley, and P. Meakin, **43**, 1134 (1991).

[29] Y. Sawada, A. Dougherty, and J. P. Gollub, Phys. Rev. Lett. **56**, 1260 (1986); D. Grier, E. Ben-Jacob, Roy Clarke, and L. M. Sander, *ibid.* **56**, 1264 (1986). For a review, see D. Kessler, J. Koplik, and H. Levine, Adv. Phys. **37**, 255 (1988).

[30] M. Leibig and T. C. Halsey (unpublished).

[31] See, e.g., W. H. Press, B. P. Flannery, S. A. Teukolsky, and W. T. Vetterling, *Numerical Recipes—The Art of Scientific Computing* (Cambridge University Press, Cambridge, 1986), Chap. 17.

[32] C. Carathéodory, *Theory of Functions of a Complex Variable* (Chelsea, New York, 1958), Vol. 1, Chap. 2.

[33] R. C. Ball, Physica A **140**, 62 (1986), and references therein. This paper also presents an argument for $D \approx 1.71$ based on the macroscopic stability of DLA clusters.

[34] J.-P. Eckmann, P. Meakin, I. Procaccia, and R. Zeitak, Phys. Rev. A **39**, 3185 (1989), and references therein.

[35] R. C. Ball and T. A. Witten, Phys. Rev. A **29**, 2966 (1984).

[36] G. A. Baker, Jr. and P. Graves-Morris, *Padé Approximants* (Addison-Wesley, Reading, MA, 1981), Vol. 1, Chap. 1.

[37] T. C. Halsey and K. Honda (unpublished).